The Reduction Pathway of End-on Coordinated Dinitrogen. I. Vibrational Spectra of Mo/W−N_2, −NNH, and −NNH_2 Complexes and Quantum Chemistry Assisted Normal Coordinate Analysis

Nicolai Lehnert and Felix Tuczek*

Institut für Anorganische Chemie und Analytische Chemie der Universität Mainz, Staudinger Weg 9, D-55099 Mainz, Germany

Received August 7, 1998

Infrared and Raman spectra of $[M(N_2)_2(dppe)_2]$ (M = W, Mo) and the two protonated derivatives $[WF(NNH)(dppe)_2]$ and $[WF(NNH_2)(dppe)_2]^+$ (dppe = 1,2-bis(diphenylphosphino)ethane) are presented. Using isotope substituted compounds (^{15}N and D) the vibrations of the Y−M−N_2H_x (x = 0, 1, 2; Y = N_2, F) central unit are identified, in particular the M−N and N−N stretching modes. In case of the monoprotonated systems, an equilibrium between metal- and nitrogen-protonated species exists that is clearly detectable in the IR spectra. Making use of theoretical force fields, a quantum chemistry assisted normal coordinate analysis (QCA-NCA) is performed for all three tungsten systems showing very good agreement with experimental frequencies. The resulting force constants for the metal−N and N−N bonds offer quantitative insight into the change of M−N and N−N bond strengths during protonation of dinitrogen bound end-on terminally to transition metals. The salient feature of this "asymmetric" protonation pathway is the strengthening of the metal−N bond going along with each protonation step whereas the N−N bond is weakened at the same time.

Introduction

Although a lot of work has been directed toward the synthesis of protonable dinitrogen complexes, the end-on terminal Mo/W−N_2 systems of type $[M(N_2)_2(P_4)]$ (P = mono- or bidentate phosphine ligands) are still unique.[1] These compounds react with mineral acids to "diazenido(−)" (NNH), "hydrazido(2−)" (NNH_2), and "hydrazidium" (NNH_3^+) intermediates which in the case of bidentate phosphine ligands can be isolated.[2] On the other hand, high yields of ammonia are obtained with monodentate phosphines. Besides the general chemical interest in understanding these reactions on a molecular level, these systems also play an important role as simple mononuclear models for nitrogenase activity. This enzyme mediates the protonation reaction of molecular dinitrogen to ammonia in the biological process of nitrogen fixation. One possible coordination of N_2 to the reactive center of nitrogenase, the FeMoCo, is the terminal end-on mode[3] which is realized in the Mo/W systems. The hypothesis exists that protonation of N_2 in the enzyme proceeds in a similar manner as in the Mo/W−N_2 complexes.[4] In that sense these systems represent the low-molecular weight models for the end-on terminal reduction and protonation pathway of nitrogenase (cf. Part II of this series).

Detailed studies on the reactivity,[1] the electrochemical,[5] and the NMR spectroscopic[6] properties of these systems have been performed. However, their vibrational properties are still largely undefined, especially those of the protonated intermediates. Correspondingly, no normal coordinate analysis has been carried out. To date, the determination of force constants has been restricted to the two-dimensional problem of the interaction between the two N−N stretches in the parent bis-dinitrogen complexes.[7] Nevertheless, the strengths of the metal−N and N−N bonds are interesting parameters as they reflect the

* Corresponding author.

(1) (a) Hidai, M.; Mizobe, Y. *Chem. Rev.* **1995**, *95*, 1115. (b) Chatt, J.; Dilworth, J. R.; Richards, R. L. *Chem. Rev.* **1978**, *78*, 589. (c) Henderson, R. A.; Leigh, G. J.; Pickett, C. J. *Adv. Inorg. Chem. Radiochem.* **1983**, *27*, 197. (d) Leigh, G. J. *Acc. Chem. Res.* **1992**, *25*, 177. (e) George, T. A.; DeBord, J. R. D. In *Molybdenum Enzymes, Cofactors and Model Systems*: Stiefel, E. I., Coucouvanis, D., Newton, W. E., eds; American Chemical Society: Washington DC, 1993.

(2) (a) Chatt, J.; Heath, G. A.; Richards, R. L. *J. Chem. Soc., Chem. Commun.* **1972**, 1010. (b) Chatt, J.; Heath, G. A.; Richards, R. L. *J. Chem. Soc., Dalton Trans.* **1974**, 2074. (c) Heath, G. A.; Mason, R.; Thomas, K. M. *J. Am. Chem. Soc.* **1974**, *96*, 260. (d) Chatt, J.; Pearman, A. J.; Richards, R. L. *J. Chem. Soc., Dalton Trans.* **1976**, 1520. (e) Chatt, J.; Pearman, A. J.; Richards, R. L. *J. Chem. Soc., Dalton Trans.* **1977**, 1852. (f) Chatt, J.; Pearman, A. J.; Richards, R. L. *J. Chem. Soc., Dalton Trans.* **1977**, 2139. (g) Chatt, J.; Pearman, A. J.; Richards, R. L. *J. Chem. Soc., Dalton Trans.* **1978**, 1766. (h) Takahashi, T.; Mizobe, Y.; Sato, M.; Uchida, Y.; Hidai, M. *J. Am. Chem. Soc.* **1980**, *102*, 7461. (i) Chatt, J.; Fakley, M. E.; Hitchcock, P. B.; Richards, R. L.; Luong-Thi, N. T. *J. Chem. Soc., Dalton Trans.* **1982**, 345. (j) George, T. A.; Tisdale, R. C. *J. Am. Chem. Soc.* **1985**, *107*, 5157. (k) Abu Bakar, M.; Hughes, D. L.; Hussain, W.; Leigh, G. J.; Macdonald, C. J.; Mohd.-Ali, H. *J. Chem. Soc., Dalton Trans.* **1988**, 2545. (l) Barclay, J. E.; Hills, A.; Hughes, D. L.; Leigh, G. J.; Macdonald, C. J.; Abu Bakar, M.; Mohd.-Ali, H. *J. Chem. Soc., Dalton Trans.* **1990**, 2503. (m) Galindo, A.; Hills, A.; Hughes, D. L.; Richards, R. L.; Hughes, M; Mason, J. *J. Chem. Soc., Dalton Trans.* **1990**, 283. (n) George, T. A.; Ma, L.; Shailh, S. N.; Tisdale, R. C.; Zubieta, J. *Inorg. Chem.* **1990**, *29*, 4789. (o) George, T. A.; Kaul, B. B.; Chen, Q.; Zubieta, J. *Inorg. Chem.* **1993**, *32*, 1706. (p) Jimenez-Tenorio, M.; Puerta, M. C.; Valerga, P.; Hughes, D. L. *J. Chem. Soc., Dalton Trans.* **1994**, 2431.

(3) (a) Deng, H.; Hoffmann, R. *Angew. Chem.* **1993**, *105*, 1125. (b) Plass, W. *J. Mol. Struc. (Theochem)* **1994**, *315*, 53.

(4) Thorneley, R. N. F.; Lowe, D. J. In *Molybdenum Enzymes*; Spiro, T. G., Ed.; John Wiley: New York, 1985.

(5) (a) Hussain, W.; Leigh, G. J.; Mohd.-Ali, H.; Pickett, C. J.; Rankin, D. A. *J. Chem. Soc., Dalton Trans.* **1984**, 1703 and references therein. (b) See also ref 7a,b.

(6) (a) Donovan-Mtunzi, S.; Richards, R. L.; Mason, J. *J. Chem. Soc., Dalton Trans.* **1984**, 469, 1329, 2429, and 2729. (b) Haymore, B. L.; Hughes, M.; Mason, J.; Richards, R. L. *J. Chem. Soc., Dalton Trans.* **1988**, 2935. (c) See also ref 7a.

10.1021/ic980939+ CCC: $18.00
Published on Web 04/01/1999

decrease in N−N and increase in M−N bond order during each protonation step. The correlation of experimental force constants to theoretical studies should further provide quantitative insight into the protonation reactions in the Mo/W systems and thus allow founded conclusions regarding the proposed asymmetric protonation pathway of nitrogenase (cf. Part II of this series).

This study concerns the vibrational properties of the two related dinitrogen complexes $[Mo(N_2)_2(dppe)_2]$ (**Ia**) and $[W(N_2)_2(dppe)_2]$ (**Ib**), both of which are structurally characterized,[8] and the two derivatives $[WF(NNH)(dppe)_2]$ (**IIb**) and $[WF(NNH_2)(dppe)_2](BF_4)$ (**IIIb**). The parent compounds **I** are very stable and can be protonated with various acids, e.g. HBF_4, to give NNH_2 complexes **III**. The NNH_2 compounds can be deprotonated, e.g. with amine-bases, to the corresponding NNH complexes **II**. Whereas the structure of the Mo−NNH_2 complex **IIIa** has been determined by X-ray crystallography,[9] no structural information is available for the Mo− and W−NNH complex **IIa** and **IIb**, respectively.[1a] In order to obtain vibrational frequencies, we performed low-temperature Raman and IR measurements of **Ia**, **Ib**, **IIb**, and **IIIb**. Due to the higher photochemical stability of the W compounds in the Raman experiments, we decided to focus in general on these systems in our spectroscopic study. By using isotope-substituted compounds (^{15}N and D), we were able to determine most frequencies of the coordinated N_2, NNH, and NNH_2 ligands. Nevertheless, the determination of reliable force constants has only been possible with the help of quantum chemistry. To this end, we performed density functional calculations on simplified model systems of **I**, **II**, and **III** (cf. Part II of this series) and used the obtained theoretical force fields as a first approximation for normal coordinate analysis. By fitting selected force constants to the measured frequencies, we arrived at a force field that is both experimentally proven and theoretically founded. This procedure is labeled quantum chemistry assisted normal coordinate analysis (QCA-NCA). The resulting force constants of the metal−N and N−N bonds are of great value to characterize the properties of the protonation pathway of end-on terminal coordinated dinitrogen and are compared in Part II to the values obtained by ab-initio theory.

Experimental and Computational Procedures

Sample Preparation, Isotopic Substitution. The dinitrogen complexes of molybdenum and tungsten with the dppe ligand as well as the derived protonated species of tungsten were prepared following literature procedures.[10] The ^{15}N isotopomer of **Ib** was synthesized using $^{15}N_2$. The further preparation of the nitrogen labeled compounds **IIb** and **IIIb** was carried out from the ^{15}N-substituted complex Ib. Deuteration of **IIIb** was achieved using CH_3OD for recrystallization. In contrast, recrystallization of the NNH complex **IIb** leads to sample decomposition. In that case, deuteration was carried out by deprotonation of deuterated **IIIb** with K_2CO_3 using D_2O and CH_3OD as solvents. Purity was checked with elemental analysis. All sample manipulations for vibrational spectroscopy were performed in a glovebox.

Raman Spectroscopy. Raman spectra were measured on a setup involving the following components: Spectra Physics 2080 Kr^+ laser; SPEX 1404 0.85 m double monochromator equipped with CCD camera (PI Instruments, 1024 × 256 pixels EEV chip) and Peltier-cooled RCA 31034 detector connected to a Stanford Research SR 400 photon counter allowing us to record spectra in spectrograph or scanning mode; liquid helium cryostat (Cryovac) for measurements from 4.2 to 300 K. The spectral bandpass was typically set at 2.0 cm^{-1}. The spectra were measured at an excitation wavelength of 647 nm; typical powers were 25 mW. Higher laser powers were found to accelerate sample decomposition. The temperature was in general kept at 20 K. Samples were pressed into the groove of a copper holder for measurement and placed into the stream of helium gas.

IR Spectroscopy. MIR and FIR spectra were obtained on CsI pellets using a Bruker IFS 66v/S FTIR spectrometer equipped with an Oxford Optistat^{CF} dynamic continuous flow helium cryostat. A DTGS detector has been employed both in the MIR and FIR region with a globar as light source. Resolution was set to 1.0 cm^{-1} in the MIR and to 1.0 or 2.0 cm^{-1} in the FIR as indicated in the figures. The spectra were recorded at 30 K.

Normal Coordinate Analysis. Normal coordinate calculations were performed using the QCPE computer program 576 by M. R. Peterson and D. F. McIntosh which involves solution of the secular equation $\boldsymbol{GFL} = \boldsymbol{\Lambda L}$ by the diagonalization procedure of Miyazawa.[11] The calculations are based on a general valence force field; force constants are refined with the nonlinear optimization routine of the simplex algorithm according to Nelder and Mead.[12] The simplex optimization always has been used to refine only *selected* force constants due to the QCA-NCA procedure.

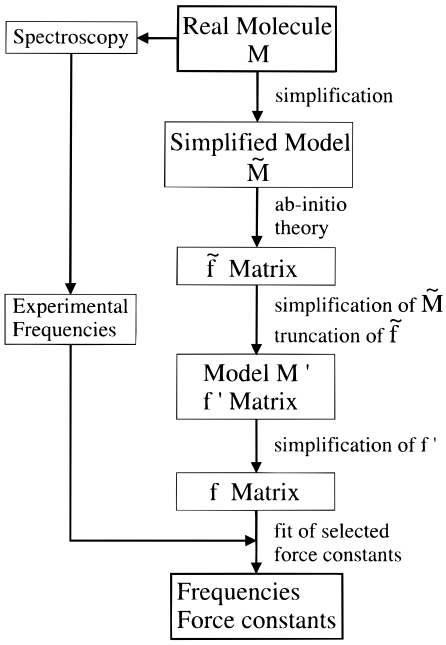

Figure 1. QCA-NCA flow chart.

Results and Analysis

A. Outline of QCA-NCA. To investigate the vibrational properties of the molecules **I**−**III**, QCA-NCA has been applied. This procedure is useful for the treatment of large molecules with normal coordinate analysis (a) if only a small number of frequencies as compared to the total number of degrees of freedom of the whole system can be safely assigned and (b) if only these few vibrations as well as their force constants are of interest. In the following, the separate steps of QCA-NCA are explained using the example of $[M(N_2)_2(dppe)_2]$ (M = Mo, W) (**I**). The procedure is illustrated in Figure 1 as a flow chart.

(7) (a) Lazarowych, N. J.; Morris, R. H.; Ressner, J. M. *Inorg. Chem.* **1986**, *25*, 3926. (b) Morris, R. H.; Earl, K. A.; Luck, R. L.; Lazarowych, N. J.; Sella, A. *Inorg. Chem.* **1987**, *26*, 2674. (c) Darensbourg, D. J. *Inorg. Chem.* **1972**, *11*, 1436. (d) Malek, A.; Folkesson, B.; Larsson, R. *Acta Chem. Scand.* **1980**, *A34*, 483.
(8) (a) Uchida, T.; Uchida, Y.; Hidai, M.; Kodama, T. *Acta Crystallogr.* **1975**, *B31*, 1197. (b) Hu, C.; Hodgeman, W. C.; Bennett, D. W. *Inorg. Chem.* **1996**, *35*, 1621.
(9) Hidai, M.; Kodama, T.; Sato, M.; Harakawa, M.; Uchida, Y. *Inorg. Chem.* **1976**, *15*, 2694.
(10) (a) Dilworth, J. R.; Richards, R. L. *Inorg. Synth.* **1980**, *20*, 119. (b) See ref 2d,e.
(11) Miyazawa, T. *J. Chem. Phys.* **1958**, *29*, 246.
(12) Nelder, J. A.; Mead, R. *Comput. J.* **1965**, *7*, 308.

Chart 1. Symbolic ***f*** Matrix of $[M(N_2)_2P_4]$ (M = Mo, W) (**I′**) in D_{2h} Symmetry[a]

	r_2	r_3	r_4	r_5	r_6	r_7	r_{68}	r_{79}	α_{24}	α_{43}	α_{35}	α_{52}
r_2	X	P_t	0	0	N_c	N_c	0	0	0	0	0	0
r_3	P_t	X	0	0	N_c	N_c	0	0	0	0	0	0
r_4	0	0	X	P_t	N_c	N_c	0	0	0	0	0	0
r_5	0	0	P_t	X	N_c	N_c	0	0	0	0	0	0
r_6	N_c	N_c	N_c	N_c	Y	N_t	N_S	N_St	0	0	0	0
r_7	N_c	N_c	N_c	N_c	N_t	Y	N_St	N_S	0	0	0	0
r_{68}	0	0	0	0	N_S	N_St	Z	NN_t	0	0	0	0
r_{79}	0	0	0	0	N_St	N_S	NN_t	Z	0	0	0	0
α_{24}	0	0	0	0	0	0	0	0	R_1	a	b_1	a
α_{43}	0	0	0	0	0	0	0	0	a	R_2	a	b_2
α_{35}	0	0	0	0	0	0	0	0	b_1	a	R_1	a
α_{52}	0	0	0	0	0	0	0	0	a	b_2	a	R_2

	α_{62}	α_{63}	α_{64}	α_{65}	α_{72}	α_{73}	α_{74}	α_{75}	lb^x_{68}	lb^y_{68}	lb^x_{79}	lb^y_{79}
α_{62}	S	c	0	0	0	d	0	0	0	0	0	0
α_{63}	c	S	0	0	d	0	0	0	0	0	0	0
α_{64}	0	0	S	c	0	0	0	d	0	0	0	0
α_{65}	0	0	c	S	0	0	d	0	0	0	0	0
α_{72}	0	d	0	0	S	c	0	0	0	0	0	0
α_{73}	d	0	0	0	c	S	0	0	0	0	0	0
α_{74}	0	0	0	d	0	0	S	c	0	0	0	0
α_{75}	0	0	d	0	0	0	c	S	0	0	0	0
lb^x_{68}	0	0	0	0	0	0	0	0	Q	0	e	0
lb^y_{68}	0	0	0	0	0	0	0	0	0	Q	0	e
lb^x_{79}	0	0	0	0	0	0	0	0	e	0	Q	0
lb^y_{79}	0	0	0	0	0	0	0	0	0	e	0	Q

[a] Top: Bonds and in-plane angles. Bottom: Out-of-plane angles and linear bends.

The real molecule **M** is too large to be handled completely with ab-initio theory and therefore must be simplified in a meaningful way leading to a model $\tilde{\mathbf{M}}$. In case of the dinitrogen complexes **I**, this is achieved by substituting the large dppe ligands with simple PH_3 groups obtaining $[M(N_2)_2(PH_3)_4]$ ($\tilde{\mathbf{I}}$) (cf. Part II of this series). In the next step, the frequencies and force constants (matrix $\tilde{f}$) of model $\tilde{\mathbf{M}}$ are calculated. For a normal coordinate analysis, further simplification of $\tilde{\mathbf{M}}$ and truncation of $\tilde{f}$ are necessary to make the problem easier to handle and remove artificial interactions. In case of $\tilde{\mathbf{I}}$, the H atoms of the introduced PH_3 ligands do not exist in the real compounds **I**, but the low-energy modes of the linear N−N−M−N−N subunit are falsified by interaction with M−P−H bending vibrations compared to the real molecule **M**. In order to eliminate these artifacts, the H atoms are removed and the model $[M(N_2)_2P_4]$ (**I′**) or, generally, **M′** is obtained.

The matrix ***f′***, obtained by truncation of the complete matrix $\tilde{f}$, can formally be divided into two parts: in case of **I′** these are (a) the force constants of the linear N−N−M−N−N unit that should be fitted to experimental frequencies (*core*) and (b) the force constants of the $[MP_4]$ unit (*frame*) that are of no immediate interest. By further neglecting small interactions it is possible to describe the frame with only a few force constants. This is meaningful because otherwise the number of frame force constants is very large without leading to an improved description of the core. Moreover, the number of nondiagonal elements between internal coordinates of the frame and the core is reduced to the largest ones. These approximations applied to the initial ***f′*** matrix of **I′** lead to the matrix ***f*** given in Chart 1 which is used for a conventional normal coordinate analysis. In the case of our study where **I**, **II**, and **III** are related, the symbolic ***f*** matrix of the frame is set up in an equivalent form for all three models **I′**−**III′**, varying only the values and the number of different force constants imposed by the lower symmetry of models **II′** and **III′**. This ensures an equivalent treatment of all three systems.

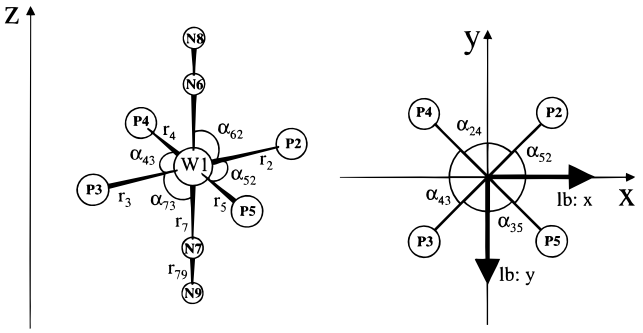

Figure 2. Internal coordinates and atomic labeling chart of model **I′**. Compare to model **Ĩa** in Part II of this series. Distances for **Ib′** (in Å): W−P = 2.454, W−N = 1.991, N−N = 1.134.

Chart 2. Definition of the Symmetry Coordinates of the Central N−N−M−N−N Unit in $[M(N_2)_2P_4]$ (M = Mo, W) (**I′**) in D_{2h}[a]

$S_1^{A_g} = \frac{1}{\sqrt{2}}(r_6 + r_7)$	ν_s(MN)
$S_2^{A_g} = \frac{1}{\sqrt{2}}(r_{68} + r_{79})$	ν_s(NN)
$S_1^{B_{2g}} = \frac{1}{\sqrt{2}}(lb^x_{68} - lb^x_{79})$	δ^x_s(MNN)
$S_1^{B_{3g}} = \frac{1}{\sqrt{2}}(lb^y_{68} - lb^y_{79})$	δ^y_s(MNN)
$S_1^{B_{1u}} = \frac{1}{\sqrt{2}}(r_6 - r_7)$	ν_{as}(MN)
$S_2^{B_{1u}} = \frac{1}{\sqrt{2}}(r_{68} - r_{79})$	ν_{as}(NN)
$S_1^{B_{2u}} = \frac{1}{\sqrt{2}}(lb^y_{68} + lb^y_{79})$	δ^y_{as}(MNN)
$S_1^{B_{3u}} = \frac{1}{\sqrt{2}}(lb^x_{68} + lb^x_{79})$	δ^x_{as}(MNN)

[a] The internal coordinates are defined in Figure 2.

In a last step, the force constants of the N−N−M−N−N core are fitted to the experimental frequencies. These belong to the internal coordinates r_6, r_7, r_{68}, r_{79}, lb^x_{68}, lb^y_{68}, lb^x_{79}, and lb^y_{79} which are defined in Figure 2. Chart 3 shows the corresponding symmetrized ***F*** matrix of the subspace of these internal coordinates (their symmetrized linear combinations are listed in Chart 2). Nondiagonal elements to frame modes are only allowed to change slightly while the frame itself is kept fixed. The results of this QCA-NCA procedure for the three different systems **Ib**, **IIb**, and **IIIb** are presented and discussed below.

B. Dinitrogen Complexes. The central N−N−M−N−N unit included in the $[M(N_2)_2P_4]$ system has eight normal modes: the symmetric and antisymmetric M−N and N−N stretches $\nu_{s/as}$(MN) and $\nu_{s/as}$(NN), respectively, and four different M−N−N linear bends, two in each orthogonal direction *x* and *y* (cf. Figure 2) labeled $\delta^x_{s/as}$(MNN) and $\delta^y_{s/as}$(MNN). The four symmetric modes are Raman active, whereas the antisymmetric ones are observed in the IR spectra. In the following, the vibrational properties of **Ib** are discussed first and then compared to those of **Ia**.

Vibrational Spectra of $[W(N_2)_2(dppe)_2]$ (Ib). The Raman spectra of **Ib** (Figure 3) exhibit four peaks at 2007, 1954, 419, and 414 cm^{-1} that shift in the ^{15}N-substituted compound (cf. Table 1a). The features at 2007 and 1954 cm^{-1} shift about 70 cm^{-1} down to 1940 and 1884 cm^{-1}, respectively, and are assigned to the N−N stretching vibrations. The symmetric, Raman active mode ν_s(NN) belongs to the intense peak at 2007 cm^{-1} whereas the Raman forbidden ν_{as}(NN) vibration is assigned to the feature at 1954 cm^{-1}. The peaks at 419 and 414 cm^{-1} both shift exactly 12 cm^{-1} on ^{15}N substitution. These features are of comparable intensity and are both assigned to the symmetric W−N stretching vibration ν_s(WN) which therefore appears to be split in the tungsten−N_2 complex **Ib**. As a consequence, none of the symmetric linear bends δ^x_s(WNN) or δ^y_s(WNN) is observed in the Raman spectra. This is in agreement with several spectroscopic studies of related com-

Chart 3. Symbolic ***F*** Matrix of the Central N−N−M−N−N Unit in $[M(N_2)_2P_4]$ (M = Mo, W) (**I′**) in D_{2h} Symmetry[a]

ν_s(MN) $A_g^{(1)}$	ν_s(NN) $A_g^{(2)}$	δ_s^x(MNN) $B_{2g}^{(1)}$	δ_s^y(MNN) $B_{3g}^{(1)}$	ν_{as}(MN) $B_{1u}^{(1)}$	ν_{as}(NN) $B_{1u}^{(2)}$	δ_{as}^y(MNN) $B_{2u}^{(1)}$	δ_{as}^x(MNN) $B_{3u}^{(1)}$
$Y + N_t$	$N_S + N_St$	0	0	0	0	0	0
$N_S + N_St$	$Z + NN_t$	0	0	0	0	0	0
0	0	$Q - e$	0	0	0	0	0
0	0	0	$Q - e$	0	0	0	0
0	0	0	0	$Y - N_t$	$N_S - N_St$	0	0
0	0	0	0	$N_S - N_St$	$Z - NN_t$	0	0
0	0	0	0	0	0	$Q + e$	0
0	0	0	0	0	0	0	$Q + e$

[a] This short form of the matrix does not include the nondiagonal element between ν_s(MN) and the totally symmetric ν_s(MP) mode ($2\sqrt{2}N_c$).

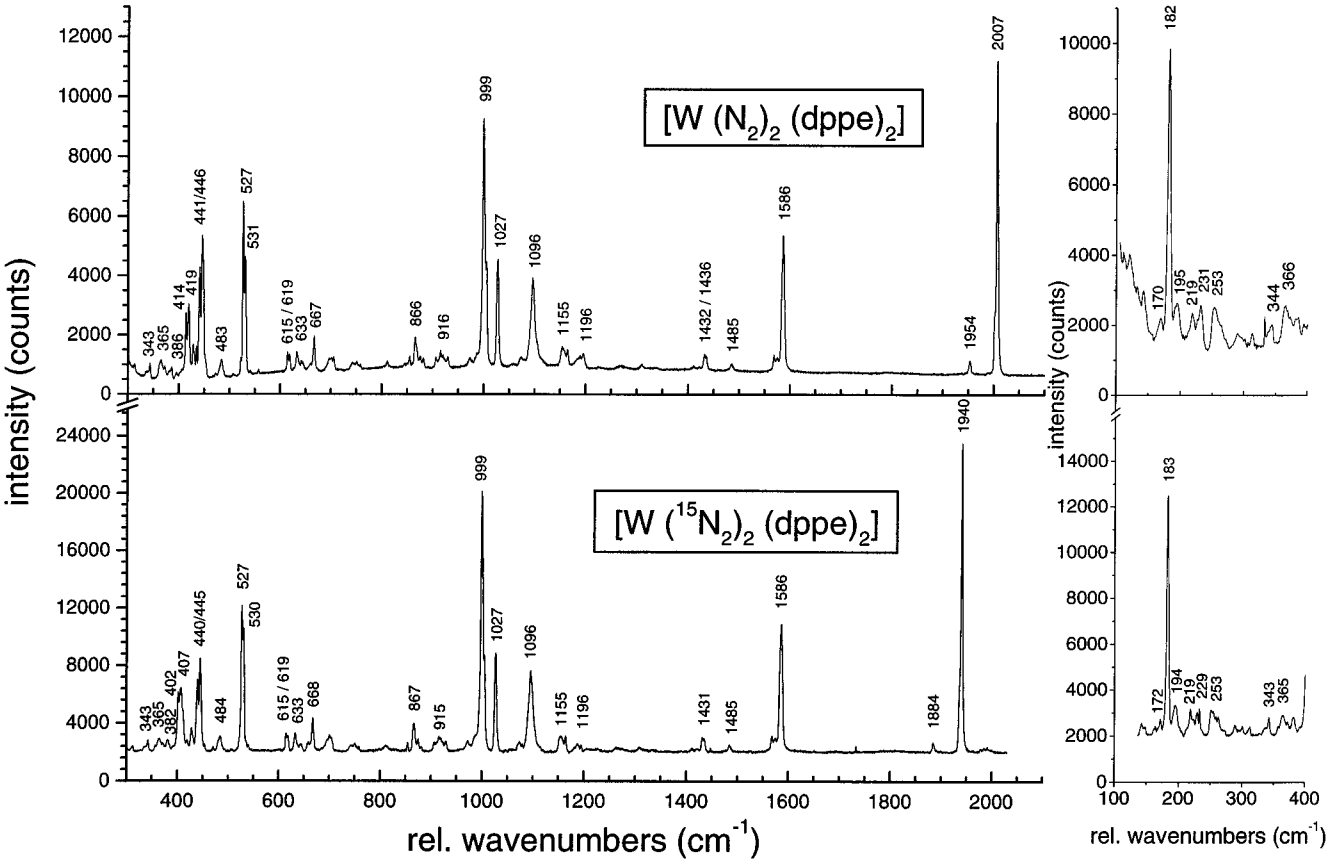

Figure 3. Raman spectra of complex **Ib** at 20 K. Top: Unlabeled complex. Bottom: ^{15}N-Substituted compound. All peak positions in cm^{-1}.

pounds which show that linear bending vibrations are of low intensity in the Raman experiment.[13,14] It is interesting to note that the forbidden mode ν_{as}(NN) has quite a large intensity. We attribute this observation as well as the splitting of ν_s(WN) to correlation effects in the solid state since compound **Ib** has a crystal structure with two molecules in the unit cell ($Z = 2$).[8] Therefore, a correlation of both ν_{as}(NN) vibrations in **Ib** formally leads to one Raman allowed and one forbidden combination. Although the gain of intensity should not be very large for the symmetric combination, we believe that this coupling mechanism may account for the intensity increase of ν_{as}(NN). While a correlation of modes in the solid state may lead to splittings up to several wavenumbers, not all modes in question are affected in the same way; i.e. some vibrations show no detectable splittings.[13] In case of **Ib**, the correlation effects are observed mainly for ν_s(WN) which is split by 5 cm^{-1} whereas ν_s(NN) only shows a slight asymmetry of the corresponding peak.

Other intense features in the Raman spectra of **Ib** (Figure 3) are found at 527, 999, 1027, 1096, and 1586 cm^{-1} which remain unshifted in the ^{15}N compound. Comparison with experimental data from $[W(N_2)_2(depe)_2]$ (depe = 1,2-bis(diethylphosphino)-ethane) (spectrum not shown) and related depe complexes of iron[14] suggests that these vibrations are due to the phenyl residues of dppe. In particular, the peak at 1586 cm^{-1} belongs to a C=C stretch; 1096 and 1027 cm^{-1} are of in-plane bending type (δ(CC) and δ(CH), respectively) and the feature at 527 cm^{-1} is either an out-of-plane bend γ(CC) or the P−phenyl stretch.[15] The peaks of medium intensity around 600 cm^{-1} are assigned to P−C stretching vibrations of the five-membered −W−P−CH_2−CH_2−P− rings. In addition, the features at 483 and about 440 cm^{-1} most probably belong to bends of these rings. In the low-energy region of the Raman spectra, a very

(13) (a) Posset, U.; Kiefer, W. *Vib. Spectrosc.* **1992**, *3*, 47. (b) Posset, U.; Kiefer, W. *J. Mol. Struct.* **1995**, *349*, 427.
(14) Tuczek, F.; Wiesler, B. E.; Lehnert, N. Unpublished results.
(15) Colthup, N. B.; Daly, L. H.; Wiberley, S. E. *Introduction to Infrared and Raman Spectroscopy*, 3rd ed.; Academic Press: Orlando, FL, 1990.

Table 1

(a) Comparison of the Observed and Calculated Frequencies of $[W(N_2)_2(dppe)_2]$ (**Ib**) (in cm^{-1})

		experimental		QCA-NCA	
mode	sym.[a]	N_2	$^{15}N_2$	N_2	$^{15}N_2$
ν_s(NN)	A_g	2007 (R)/ 2009 (IR)[b]	1940 (R)/ 1942 (IR)	2007	1940
ν_{as}(NN)	B_{1u}	1954 (R)/ 1948 (IR)	1884 (R)/ 1883 (IR)	1948	1883
δ_{as}(WNN)	B_{2u}/B_{3u}	555 (IR)	538 (IR)	556	538
ν_{as}(WN)	B_{1u}	435 (IR)		435	424
ν_s(WN)	A_g	419/414 (R)	407/402 (R)	420	406
δ_s(WNN)	B_{2g}/B_{3g}			462	447
ν(WP)	B_{2u}/B_{3u}	236/204 (IR)	236/204 (IR)	(∼295)	(∼295)
ν_s(WP)	A_g	182 (R)	183 (R)		

(b) Observed Frequencies of $[Mo(N_2)_2(dppe)_2]$ (**Ia**) and $[Mo(N_2)_2(dppe)_2]\cdot[MoCl_2(dppe)_2]$ (**IV**) (in cm^{-1})

		experimental	
mode	sym.[a]	**Ia**	**IV**
ν_s(NN)	A_g	2033 (R)/2039 (IR)[b]	2038 (R)/2039 (IR)
ν_{as}(NN)	B_{1u}	1980 (IR)	1980 (IR)
δ_{as}(MoNN)	B_{2u}/B_{3u}	550 (IR)	546/539 (IR)
ν_s(MoN)	A_g	393/(404) (R)	389 (R)

[a] Symmetry labels according to D_{2h} of **I′**. [b] Data from Raman or IR spectroscopy, respectively.

intense peak is observed at about 180 cm^{-1} which is assigned to the symmetric W−P stretch ν_s(WP) (cf. Table 1a) in accordance with results of Posset et al. on $[Mo(CO)_4(dppe)]$.[13]

The IR spectra of complex Ib are given in Figure 4. Besides the N−N stretching vibrations ν_s(NN) (IR forbidden) at 2009 cm^{-1} and ν_{as}(NN) (allowed) at about 1948 cm^{-1} which shift on ^{15}N substitution to 1942 and 1883 cm^{-1}, respectively, two other isotope sensitive peaks are found below 600 cm^{-1}. The peak at 555 cm^{-1} is assigned to both antisymmetric linear bends δ^x_{as}(WNN) and δ^y_{as}(WNN) which obviously have the same frequency and shift to 538 cm^{-1} in the ^{15}N compound. In contrast, the analogous depe complex shows a splitting of the linear bends of 9 cm^{-1} in the IR spectrum (data not shown) but the reason for the occurrence (or vice versa the absence) of this splitting is not clear. A similar problem arises for **Ia** (see below). In the spectral region from 350 to 450 cm^{-1} numerous features are observed making unequivocal assignments difficult. Nevertheless, the distinct change in the overall appearance of the spectrum on ^{15}N substitution leads to the conclusion that an isotope sensitive vibration must be present in this region which is coupled to other modes. This vibration can only be the antisymmetric W−N stretch ν_{as}(WN) which most reasonably is identified with the medium intense peak at 435 cm^{-1} that disappears in the ^{15}N compound. Below 300 cm^{-1} there are two features of low intensity at 236 and 204 cm^{-1} which are assigned to the odd W−P stretching vibrations. The complete assignments are listed in Table 1a. The intense peaks at 1586, 1571, 1484, and 1432 cm^{-1} clearly belong to four C═C stretching modes of the phenyl residues.[15]

It is interesting to note that ν_{as}(NN) is very broad in the IR spectra in contrast to the Raman data and appears to be split both in the dppe (cf. Figure 4) and depe complex (spectrum not shown). The reason for this, however, is not clear and may be attributed to effects of the CsJ matrix.

Table 1b shows the Raman and IR data (spectra not shown) of **Ia** and of cocrystallized material of **Ia** and $[MoCl_2(dppe)_2]$ (about 1:1, **IV**). The symmetric Mo−N stretch appears at 389 cm^{-1} in **IV** and at 393 cm^{-1} in **Ia**. Moreover, an additional feature at 404 cm^{-1} is found in the Raman spectrum of **Ia** which is missing both in **IV** and pure $[MoCl_2(dppe)_2]$ (data not shown). Maybe this peak also belongs to ν_s(MoN) which therefore appears to be split in **Ia** due to correlation effects in the solid state as observed for Ib (see above). However, this is in contrast to the X-ray data of **Ia**[8] which indicate a structure with only one molecule per unit cell ($Z = 1$). The cocrystallized material exhibits a splitting of the antisymmetric bending vibrations δ_{as}(MoNN) appearing at 546 and 539 cm^{-1}, whereas for the pure compound **Ia** only one peak at 550 cm^{-1} occurs.

QCA-NCA of $[W(N_2)_2(dppe)_2]$. The spectroscopic investigation of **Ib** has led to the assignment of eight vibrations. Table 1a gives the frequencies obtained for **Ib** with the QCA-NCA procedure, and Table 2 comprises the corresponding force constants in internal coordinates. Force constants of the $[MP_4]$ frame which are not fitted are indicated. In case of the N−N stretching vibrations, the symmetric mode is fitted to the Raman and the antisymmetric one to the IR data. Altogether very good agreement with experiment is achieved.

Importantly, the ab-initio force fields of **Ĩa** and **Ĩb** (symmetry D_{2h}) predict a splitting of the antisymmetric linear bends δ_{as}(MNN) of about 10 cm^{-1} which results (a) mainly from an unequal coupling of the linear bends to octahedral bends of type δ(PMN) and (b) from a slight difference in the force constants Q and e for the x and y direction of the linear bending motion. It is not clear why in certain cases a splitting of the linear bends is observed experimentally. In view of these uncertainties, it appears most reasonable to treat both linear bends as equivalent. This is achieved by setting the small couplings to the octahedral bends to zero and by using only one set of force constants Q and e (cf. Charts 1 and 3). Another problem lies in the fact that the symmetric linear bends could not be identified in the Raman spectra. Based on the calculations, the off-diagonal element e (cf. Chart 3) is estimated to about 0.1, and the calculated energy of δ_s(WNN) is only listed for comparison. In the spirit of the QCA-NCA approach, the frequencies of the W−P stretches are not fitted as these modes belong to the frame. They are predicted to appear at distinctly higher energy than experimentally observed due to the absence of the residues at the phosphorus atoms in the model systems (two phenyl groups and one ethyl bridge). Most probably, this also accounts for the large energetic separation between the different W−P stretches as observed in the spectra which is missing in the calculation.

C. NNH_2 Complex of W. The model $[WF(NNH_2)P_4]$ (**IIIb′**) has a planar W−NNH_2 subunit and therefore C_{2v} symmetry. The structure of **IIIb′** is given in Figure 5. The corresponding central F−W−N−NH_2 core has 11 normal modes: five stretches ν(WF), ν(WN), ν(NN), and $\nu_{s/as}$(NH); two N−N−H bends $\delta_{s/as}$(NNH) and two linear bends $\delta^{y/x}$(WNN); one out-of-plane bend γ at N_8; and a torsion τ around the W−N−NH_2 axis. All these vibrations are Raman active in C_{2v} and, with exception of the torsion, IR allowed. Unfortunately, the Raman spectra of IIIb (data not shown) are almost featureless. Therefore, our vibrational analysis is exclusively based on the IR spectra of this system.

IR Spectra of $[WF(NNH_2)(dppe)_2](BF_4)$ (IIIb). The IR spectra of **IIIb** including isotopically labeled compounds (Figure 6) exhibit seven peaks that distinctly shift on isotopic substitution. The two N−H stretching vibrations are clearly identified at 3335 (ν_{as}(NH)) and 3258 cm^{-1} (ν_s(NH)). Both show a strong shift on deuteration down to 2500 and 2389 cm^{-1}, respectively. The assignment of ν_{as}(NH) to the feature at higher energy is in accordance with the ab-initio calculation presented in Part II of this series. A third, much broader peak at about 3175 cm^{-1} which also appears to shift on deuteration may be due to

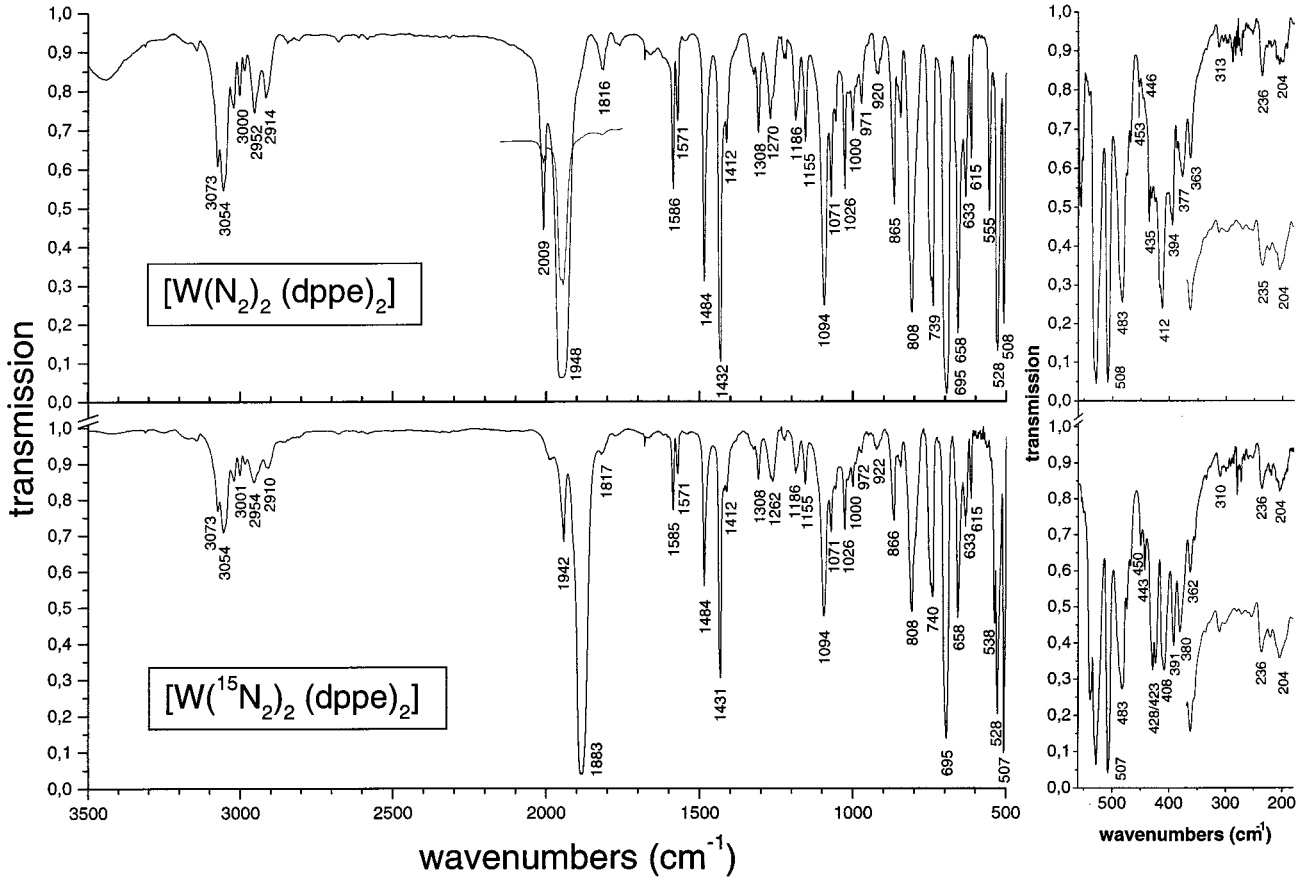

Figure 4. IR spectra of complex **Ib** at 30 K. Top: Unlabeled complex. Bottom: ^{15}N-Substituted compound. All peak positions in cm^{-1}. In the FIR region, spectra were recorded using a 12 μm Mylar beamsplitter with resolution set to 1 cm^{-1}. The inserted data were measured with 6 μm Mylar and 2 cm^{-1} resolution.

Table 2. Force Constants of the Internal Coordinates (***f*** Matrix) of $[W(N_2)_2(dppe)_2]$ (**Ib**)

force constant[a]		complex **Ib**	free N_2
X	f[b]	1.3831	
P_t	f	0.1979	
R_1	f	0.6848	
R_2	f	0.5184	
a	f	−0.1450	
b_1	f	−0.3948	
b_2	f	−0.2284	
S	f	0.4316	
c	f	−0.1870	
d	f	−0.2327	
Y		2.65505	
N_t		0.27965	
Z		16.43148	22.42[c]
NN_t		0.27738	
N_S		0.95744	
N_St		−0.13024	
Q		0.69955	
e[d]		0.09955	
N_c[e]		0.02965	

[a] Units are mdyn/Å for stretching, mdyn·Å for bending, and mdyn for stretch−bend interactions. [b] "f" indicates a frame force constant. [c] Calculated with a harmonic force field. [d] Approximately set to ∼0.1. [e] N_c is the only nondiagonal element between frame and core internals and therefore only slightly changed (initial value: 0.0368).

hydrogen bridges of the N−H groups with BF_4^- ions. Such interactions are in fact present in the solid state as evidenced by the X-ray structure of $[MoF(NNH_2)(dppe)_2](BF_4)$ (**IIIa**)[9] and partly could be conserved in the CsJ pellet. The symmetric N−N−H bending vibration is assigned to the peak at 1601 cm^{-1}

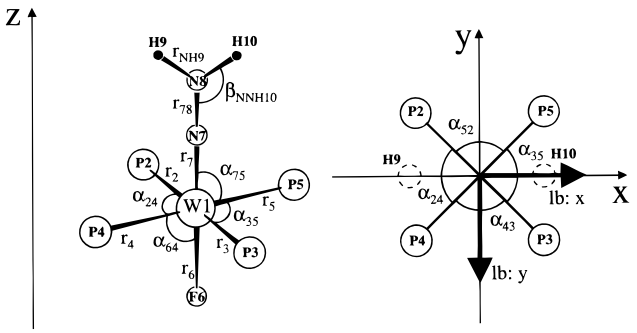

Figure 5. Internal coordinates and atomic labeling chart of model **IIIb′**. Compare to model **IÎIa** in Part II of this series. Distances for **IIIb′** (in Å): W−P = 2.540, W−N = 1.763, N−N = 1.332, W−F = 1.990, N−H = 1.090; angle: N−N−H = 125°.

which should shift below 1200 cm^{-1} on deuteration based on the ab-initio calculation. This mode is identified with the shoulder at 1181 cm^{-1} appearing in the deuterated compound, but it is equally possible that the deuterium shifted peak is masked by the strong absorptions below 1160 cm^{-1}. Unfortunately, the corresponding antisymmetric mode could not be identified in the spectra.[16] In the ^{15}N-substituted compound, the three observed N−H vibrations ($\nu_{s/as}$(NH) and δ_s(NNH)) show small shifts below 10 cm^{-1}.

In the region between 1500 and 500 cm^{-1} are two isotope sensitive features at 1387 and 581 cm^{-1} which are assigned to

(16) Although one should be very careful when interpreting the calculated IR intensities, it is striking that ab-initio theory predicts an intensity for this mode which is close to zero. Therefore, the absence of this vibration in the IR spectra appears plausible.

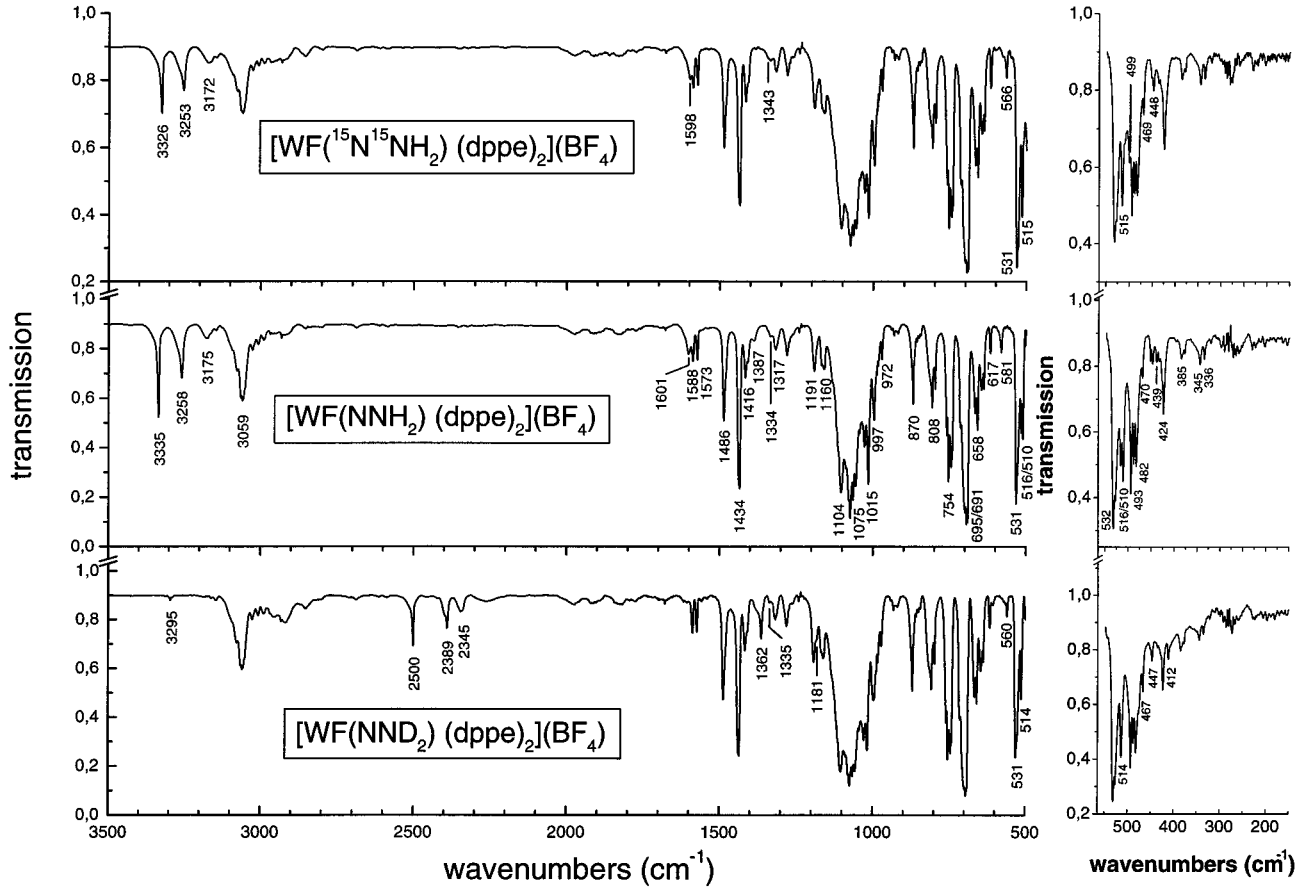

Figure 6. IR spectra of complex **IIIb** at 30 K. Top: ^{15}N-Substituted compound. Middle: Unlabeled complex. Bottom: ^{2}H-Substituted compound. All peak positions in cm^{-1}. In the FIR region, spectra were recorded using a 12 μm Mylar beamsplitter with resolution set to 1 cm^{-1}.

the N−N and W−N stretching vibrations ν(NN) and ν(WN), respectively. The small peak at 1387 cm^{-1} is distinctly missing in both labeled compounds. The ^{15}N substituted complex shows an additional feature at 1343 cm^{-1} of comparable intensity which almost merges with the 1334 cm^{-1} peak. In case of the deuterated complex, a more intense feature occurs at 1362 cm^{-1}. This gain of intensity and the relatively large shift on deuteration are due to strong mixing of ν(NN) with ν_s(NH) (see QCA-NCA results). In case of ν(WN), the isotope shifted peaks are clearly identified at 566 (^{15}N) and 560 cm^{-1} (^{2}H), respectively (cf. Figure 6). The very intense features at about 1070 cm^{-1} belong to the B−F stretching mode of T_2 symmetry (in T_d) of the BF_4^- ions.

The low-energy region contains two more peaks that shift upon isotope substitution. The feature at 510 cm^{-1} is assigned to the linear bend δ^y(WNN) the motion of which is directed out of the NNH_2 plane. The corresponding peak in the ^{15}N compound is at 499 cm^{-1}. The much higher intensity of this bend in the unlabeled complex is due to strong mixing with the more intense mode at about 515 cm^{-1}. Therefore, it is difficult to decide whether the 516 or 510 cm^{-1} feature has more bending character. The above assignment is based on the isotopic shift expected from NCA. In the deuterated compound, this vibration cannot be observed and is most probably masked by the strong features at about 490 cm^{-1}. At 439 cm^{-1} a peak of very low intensity occurs which shifts to 412 cm^{-1} upon deuteration and is absent in the ^{15}N compound. This feature is assigned to the linear bend δ^x(WNN) and not to the out-of-plane mode γ, because γ should exhibit a much larger shift on deuteration as predicted by the ab-initio calculation. The assignment of the W−F stretching vibration is difficult, because this mode should be less sensitive to isotopic substitution. One candidate is the peak at 470 cm^{-1} which shifts to 469 and 467 cm^{-1} on ^{15}N and ^{2}H substitution, respectively. Tentatively we assign ν(WF) to this feature.

QCA-NCA of [WF(NNH$_2$)(dppe)$_2$](BF$_4$). The structure of model system [WF(NNH_2)P_4] (**IIIb′**) is chosen in accordance to **I′** with an orthogonal [WP_4] frame (D_{4h} symmetry). Since the crystal structure of **IIIb** is unknown, all bond lengths are taken from the X-ray structure of the Mo analogon [MoF(NNH_2)(dppe)$_2$](BF_4) (**IIIa**),[9] but with an average M−P distance as in the case of **I′**. The obtained model **IIIb′** has C_{2v} symmetry and is depicted in Figure 5 along with the definition of the internal coordinates. The ***f*** matrix of **IIIb′** is set up according to the QCA-NCA procedure (see Section A) with all ab-initio force constants taken from the calculation of **IĨIa**. Furthermore, in analogy to **I′**, all nondiagonal elements between the linear bends $\delta^{x/y}$(WNN) and octahedral bends δ(PWF) and δ(PWN), respectively, are set to zero. The resulting ***F*** matrix of the F−W−N−NH_2 core in symmetrized internals (cf. Chart 4) is given in Chart 5.

Table 3 contains the results for model **IIIb′** obtained with the QCA-NCA procedure showing very good agreement with experiment; the corresponding force constants are given in Table 4. In contrast to the dinitrogen systems (Section B), the spectroscopic information is less complete in the present case. The fact that for some modes not all three isotopic peaks are observed in the spectra would present a serious problem for a conventional NCA. In contrast, the QCA-NCA procedure is based on an ab-initio force field and theoretical shifts can be used for assignments (see above). Nevertheless, the significance of the results suffers from this lack of spectroscopic information

Chart 4. Definition of the Symmetry Coordinates of the Central F−W−N−NH_2 Unit in [WF(NNH_2)P_4] (**IIIb′**) in C_{2v}[a]

$S_1^{A_1}=r_6$	ν(WF)
$S_2^{A_1}=r_7$	ν(WN)
$S_3^{A_1}=r_{78}$	ν(NN)
$S_4^{A_1}=\frac{1}{\sqrt{2}}(r_{NH_9}+r_{NH_{10}})$	ν_s(NH)
$S_5^{A_1}=\frac{1}{\sqrt{2}}(\beta_{NNH_9}+\beta_{NNH_{10}})$	δ_s(NNH)
$S_1^{A_2}=\tau_{W-N-NH_2}$	τ
$S_1^{B_1}=\frac{1}{\sqrt{2}}(r_{NH_9}-r_{NH_{10}})$	ν_{as}(NH)
$S_2^{B_1}=\frac{1}{\sqrt{2}}(\beta_{NNH_9}-\beta_{NNH_{10}})$	δ_{as}(NNH)
$S_3^{B_1}=lb_{78}^x$	δ^x(WNN)
$S_1^{B_2}=\gamma_{NNH_2}$	γ
$S_2^{B_2}=lb_{78}^y$	δ^y(WNN)

[a] The internal coordinates are defined in Figure 5.

(cf. Table 3). This applies to the symmetric N−N−H bend, the frequency of which cannot unequivocally be identified in the spectrum of the deuterated compound (see above). In view of this uncertainty, the assignment to the shoulder appearing at 1181 cm^{-1} is used for NCA, but only with a low weight during the fit. If all nondiagonal elements are set to zero, the shift of δ_s(NNH) on deuteration is 120 cm^{-1} too large. By fitting the A_1 block of the ***F*** matrix the error is reduced to 13 cm^{-1}, but further reduction leads to a deterioration of the fit of the other frequencies. In view of the uncertain assignment, this is not desirable. Since the corresponding antisymmetric bend δ_{as}(NNH) is not observed, the experimental deuterium shifts of the bends are unknown and cannot be used to assess the ab-initio results. The frequency of δ_{as}(NNH) is reasonably estimated leaving the force constant H_{Bt} at its initial value predicted by theory. This also applies to the nondiagonal element $H_{SB} - H_{SBt}$, although an improvement for the fit of ν_{as}(NH) could be achieved by varying this matrix element. Nevertheless, this would not be meaningful because of the unknown frequency of δ_{as}(NNH).

The very large shifts of both ν(NN) and ν(WN) on deuteration are correctly reproduced by the NCA by coupling both modes to ν_s(NH) (matrix elements H_{NN}^S and H_{MN}^S, respectively). Furthermore, the matrix element H_{NN}^B coupling ν(NN) to the symmetric bend δ_s(NNH) is large. This is similar to results obtained on a trans-diazene complex of iron.[18] The nondiagonal element connecting δ^y(WNN) and γ is only slightly changed and the diagonal force constants of the unobserved modes τ and γ are completely held fixed during the NCA fit.

D. NNH Complex of W. The model [WF(NNH)P_4] (**IIb′**) has C_s symmetry with a bent W−NN subunit as shown in Figure 7. The F−W−NNH core has eight normal modes: four stretches ν(WF), ν(WN), ν(NN), and ν(NH); two bends δ(WNN) and δ(NNH); and two torsions τ(NN) and τ(WN). All these vibrations are Raman and IR active in C_s. As observed for **IIIb**, the Raman spectra of **IIb** (data not shown) are almost featureless, thus making IR spectroscopy the only source of information for the vibrational properties of this system.

IR Spectra of [WF(NNH)(dppe)$_2$] (IIb). Figure 8 contains the infrared spectra of **IIb** and the corresponding isotope-labeled compounds. In the MIR region two isotope sensitive peaks are observed at 1457 and 1222 cm^{-1}, which shift to 1406 and 1208 cm^{-1} on ^{15}N substitution. These features are assigned to ν(NN) and δ(NNH), respectively. In the deuterated compound, ν(NN) is found at 1419 cm^{-1} and the N−N−D bend is identified with the new feature at 984 cm^{-1}. Nevertheless, it appears that the material is not completely deuterated because the signal of the unlabeled δ(NNH) bend at 1222 cm^{-1} has not completely disappeared. Unfortunately, the N−H stretching vibration cannot be assigned from the spectra. The same applies to ν(WN) which possibly is masked by the strong absorption at about 530 cm^{-1}. On isotope substitution, this feature shows a slight shift to lower wavenumbers which may be due to an underlying peak that is isotope sensitive. Therefore, ν(WN) is set to 530 cm^{-1}.

In the FIR region, only one feature is observed at 514 cm^{-1} that shows an isotope shift down to 502 cm^{-1} on ^{15}N substitution. In the deuterated complex, no corresponding peak is observed. Most reasonably this feature is assigned to δ(WNN) which exhibits a large shift on deuteration and probably is masked by the intense peaks at about 480 cm^{-1} in that compound. As in the case of **IIIb** (see above), the assignment of ν(WF) is difficult, because this mode is less isotope sensitive. One possible candidate is the peak at 459 cm^{-1} which is of similar intensity and close in energy to the corresponding feature of **IIIb**. Tentatively, we assign ν(WF) to this peak. Careful examination of the FIR spectra for both torsional modes remains unsuccessful.

It is very interesting to compare the IR spectrum of [WF(NNH)(dppe)$_2$] with that of the analogous bromo complex exhibiting a very intense absorption at 1874 cm^{-1} (Figure 9). Moreover, the peak corresponding to ν(NN) of **IIb** is missing in the region from 1300 to 1600 cm^{-1}. Obviously, this compound is *metal protonated*. Therefore, the peak at 1874 cm^{-1} is assigned to ν(NN) of a seven-coordinate compound formulated as [WHBr(N_2)(dppe)$_2$]. The corresponding W−H stretch should be of lower intensity and cannot be identified in the spectrum. Maybe this feature is masked by the strong and relatively broad ν(NN) absorption. A closer examination of the spectral region around 1800 cm^{-1} in the fluoro complex **IIb** reveals that this compound also contains small amounts of the corresponding metal-protonated species. The peak at 1846 cm^{-1} shifts down to 1761 cm^{-1} on ^{15}N substitution and remains unshifted on deuteration. Therefore, this feature is assigned to ν(NN) in the seven-coordinate complex [WHF(N_2)(dppe)$_2$]. The W−H stretching vibration is assigned to the small peak at 1811 cm^{-1} which is distinctly missing in the ^2H substituted compound. This feature should appear at about 1300 cm^{-1} on deuteration, but it is difficult to find the shifted peak in the spectrum because of its low intensity. Maybe it is associated with the small shoulder appearing on the low energy side of the 1312 cm^{-1} feature. The complete assignments are collected in Table 5.

These results are in agreement with the finding of Chatt et al.[19] that for the monoprotonated systems an equilibrium between nitrogen and metal-protonated complexes exists

$$[MX(NNH)(P)_4] \rightleftharpoons [MHX(N_2)(P)_4]$$

that depends on the nature of X (and on the nature of M and $(P)_4$, too). It is possible to determine the position of this equilibrium by IR spectroscopy. While in case of the fluoro complex **IIb** only small amounts of metal-protonated species appear, the equilibrium lies completely on the side of metal protonation for the bromo compound.

QCA-NCA of [WF(NNH)(dppe)$_2$]. Since no X-ray structure of a diazenido(−) complex **II** is available, the geometry of model [WF(NNH)P_4] (**IIb′**, C_s symmetry) is derived from the optimized structure of the Mo analogon [MoF(NNH)(PH_3)$_4$] (**IIa**, cf. Part II of this series) with a bent W−NN subunit as

(17) Jensen, H. J. A.; Jørgensen, P.; Helgaker, T. *J. Am. Chem. Soc.* **1987**, *109*, 2895.
(18) Lehnert, N.; Wiesler, B. E.; Tuczek, F.; Hennige, A.; Sellmann, D. *J. Am. Chem. Soc.* **1997**, *119*, 8879.
(19) Chatt, J.; Kan, C. T.; Leigh, G. J.; Pickett, C. J.; Stanley, D. R. *J. Chem. Soc., Dalton Trans.* **1980**, 2032.

Chart 5. Symbolic ***F*** Matrix of the Central F−W−N−NH_2 Unit in [WF(NNH_2)P_4] (**IIIb′**) in C_{2v} Symmetry[a]

ν(WF) $A_1^{(1)}$	ν(WN) $A_1^{(2)}$	ν(NN) $A_1^{(3)}$	ν_s(NH) $A_1^{(4)}$	δ_s(NNH) $A_1^{(5)}$	τ $A_2^{(1)}$	ν_{as}(NH) $B_1^{(1)}$	δ_{as}(NNH) $B_1^{(2)}$	δ^x(WNN) $B_1^{(3)}$	γ $B_2^{(1)}$	δ^y(WNN) $B_2^{(2)}$
Y_1	N_t	N_SF	0	0	0	0	0	0	0	0
N_t	Y_2	N_S	$\sqrt{2}H^S_{MN}$	$\sqrt{2}H^B_{MN}$	0	0	0	0	0	0
N_SF	N_S	Z	$\sqrt{2}H^S_{NN}$	$\sqrt{2}H^B_{NN}$	0	0	0	0	0	0
0	$\sqrt{2}H^S_{MN}$	$\sqrt{2}H^S_{NN}$	$H_S + H_St$	$H_{SB} + H_{SB}t$	0	0	0	0	0	0
0	$\sqrt{2}H^B_{MN}$	$\sqrt{2}H^B_{NN}$	$H_{SB} + H_{SB}t$	$H_B + H_Bt$	0	0	0	0	0	0
0	0	0	0	0	T	0	0	0	0	0
0	0	0	0	0	0	$H_S - H_St$	$H_{SB} - H_{SB}t$	0	0	0
0	0	0	0	0	0	$H_{SB} - H_{SB}t$	$H_B - H_Bt$	0	0	0
0	0	0	0	0	0	0	0	Q_2	0	0
0	0	0	0	0	0	0	0	0	G	G_{lb}
0	0	0	0	0	0	0	0	0	G_{lb}	Q_1

[a] This short form of the matrix does not include the nondiagonal elements between ν(WF) and ν(WN) and the totally symmetric ν_s(WP) mode ($2F_c$ and $2N_c$, respectively).

Table 3. Comparison of the Observed and Calculated Frequencies of [WF(NNH_2)(dppe)$_2$](BF_4) (**IIIb**) (in cm^{-1})

		experimental[b]			QCA-NCA		
mode	sym.[a]	NNH_2	$^{15}N^{15}NH_2$	NND_2	NNH_2	$^{15}N^{15}NH_2$	NND_2
ν_{as}(NH)	B_1	3335	3326	2500	3341	3332	2471
ν_s(NH)	A_1	3258	3253	2389	3259	3252	2383
δ_s(NNH)	A_1	1601	1598	(1181)	1602	1598	1168
ν(NN)	A_1	1387	1343	1362	1387	1342	1364
δ_{as}(NNH)	B_1				1245	1233	997
ν(WN)	A_1	581	566	560	582	567	558
δ^y(WNN)	B_2	(516)/ 510	499		511	498	484
ν(WF)	A_1	470	469	467	470	470	470
δ^x(WNN)	B_1	439		412	441	430	407
γ	B_2				271	268	214
τ	A_2				105	105	74
ν(WP)					∼230	∼230	∼230[c]

[a] Symmetry labels according to C_{2v} of **IIIb′**. [b] Data from IR spectroscopy. [c] The B_2 mode is shifted to 249 cm^{-1} by interaction with γ.

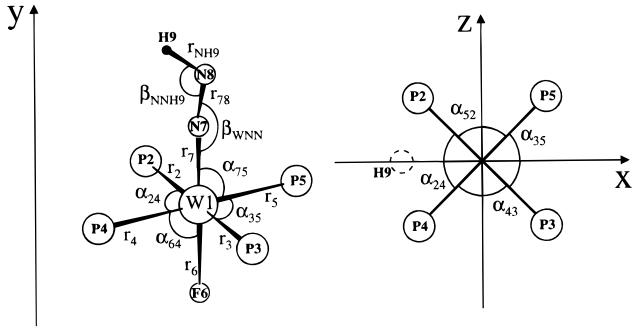

Figure 7. Internal coordinates and atomic labeling chart of model **IIb′**. Compare to model **IIa** in Part II of this series. Distances for **IIb′** (in Å): W−P = 2.540, W−N = 1.826, N−N = 1.276, W−F = 2.070, N−H = 1.050; angles, W−N−N = 170°, N−N−H = 115°.

depicted in Figure 7. In accordance with **I′** and **IIIb′**, the [WP_4] frame is chosen to be orthogonal with averaged W−P distances. The ***f*** matrix of **IIb′** is based on the calculated force constants of **IIa**. Couplings between octahedral bends (δ(PWF) and δ(PWN)) and core vibrations are neglected except for δ(WNN). In that case the interaction is very strong and nondiagonal elements α and β[20] (cf. Chart 7) are necessary to fit this mode with reasonable force constants. Chart 6 comprises the symmetrized internals, and the corresponding ***F*** matix of the core modes is given in Chart 7.

With only four of 8 normal modes identified for **IIb**, a full normal coordinate analysis cannot be applied to **IIb′**. Instead, only a few force constants of the ab-initio force field are varied to reproduce the experimental frequencies. It is unfortunate that the W−N stretch could not be observed as the position of this mode strongly influences both ν(NN) and δ(WNN). Therefore,

Table 4. Force Constants of the Internal Coordinates (***f*** Matrix) of [WF(NNH_2)(dppe)$_2$](BF_4) (**IIIb**) and [WF(NNH)(dppe)$_2$] (**IIb**)

IIIb			**IIb**		
force constant[a]	complex **IIIb**	free NNH_2[b]	force constant[a]		complex **IIb**
Y_1	2.27000		Y_1	a[c]	2.1668
Y_2	6.31097		Y_2	a	4.4860
N_t	0.46833		N_t		0.3659
Z	7.19748	11.66	Z	ft	8.27202
N_S	0.63779		N_S		0.7744
N_SF	0.20100		N_SF		0.1567
H_S	6.00549	5.89/4.61	H_S		6.0251
H_St	−0.04666	0.36	HN		0.1155
			NS		
H^S_{NN}	−0.26963	1.11/1.07	H^S_{MN}		−0.1352
H^S_{MN}	0.14190				
			H_B	ft	0.85353
H_B	1.24824	1.49/1.47	H^B_{NN}	ft	0.65975
H_Bt	0.46480	0.58	H^B_{MN}		−0.0376
H^B_{NN}	0.47921	0.59	H_{SB}		0.2796
H^B_{MN}	0.02488				
H_{SB}	−0.07134	−0.25/−0.19	H_M	ft	0.53123
$H_{SB}t$	−0.15524	−0.23/−0.26	H^M_{MN}		0.2180
			H^M_{MM}	a	0.1546
G	0.04330	(0.91)	H^M_{MH}		0.0383
Q_1	0.38961		H_{MB}	ft	0.08000
Q_2	0.69387				
G_{lb}	−0.06119		T_1		0.0426
			T_2		0.0342
T	0.01030		T_{12}		0.0276
N_c[d]	0.04099		N_c1/N_c2[e]		0.0550/0.0504
F_c[d]	0.06270		F_c1/F_c2[e]		0.0405/0.0444

[a] Units are mdyn/Å for stretching, mdyn·Å for bending, and mdyn for stretch−bend interactions. [b] Calculated force field for free isodiazene[17] with a distorted structure. [c] "a" indicates an adjusted force constant and "ft" a fitted force constant (see text). [d] N_c and F_c are the only nondiagonal elements between frame and core internals; N_c is slightly changed (initial value: 0.0431). [e] N_c1, N_c2 and F_c1, F_c2 are nondiagonal elements between frame and core internals.

it is necessary to estimate the diagonal force constant Y_2 of ν(WN). The results from spectroscopy suggest that the W−N stretch appears somewhere near 530 cm^{-1} (see above). Accordingly, the first step of our procedure is to adjust the diagonal element Y_2 of ν(WN) to reproduce the supposed frequency of 530 cm^{-1}. This way, ν(WN) and δ(WNN) get much closer in energy than predicted by the ab-initio force field and it becomes necessary to increase their nondiagonal element H^M_{MM} in order to correctly reproduce the observed isotope shift of δ(WNN). Finally, ν(WF) is set to 459 cm^{-1} by changing its diagonal element Y_1. After adjusting these three force constants the second step is to fit the observed modes ν(NN), δ(WNN) and δ(NNH) by varying their diagonal force constants Z, H_M and H_B, and

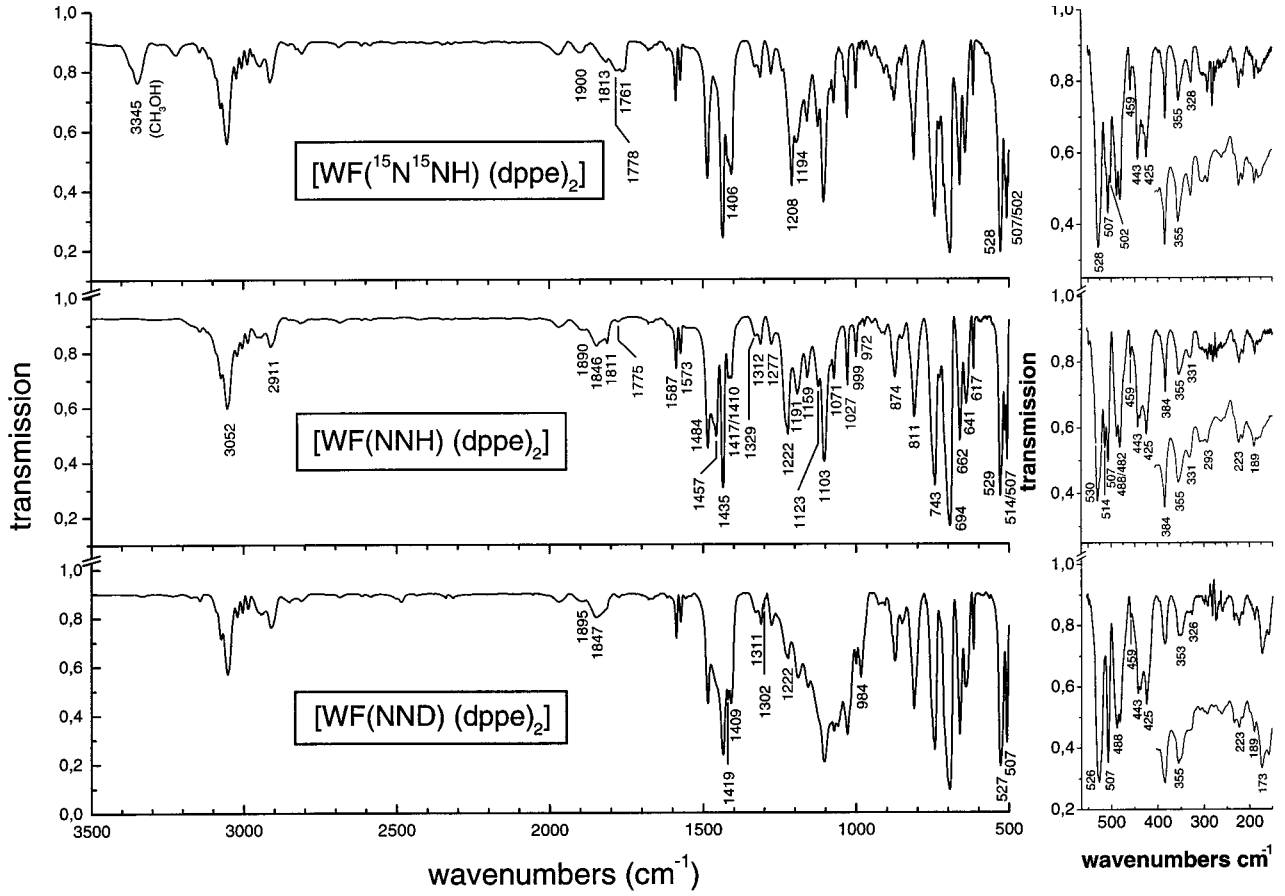

Figure 8. IR spectra of complex **IIb** at 30 K. Top: ^{15}N-Substituted compound. Middle: Unlabeled complex. Bottom: ^{2}H-Substituted compound. All peak positions in cm^{-1}. In the FIR region, spectra were recorded using a 12 μm Mylar beamsplitter with resolution set to 1 cm^{-1}. The inserted data were measured with 6 μm Mylar and 2 cm^{-1} resolution.

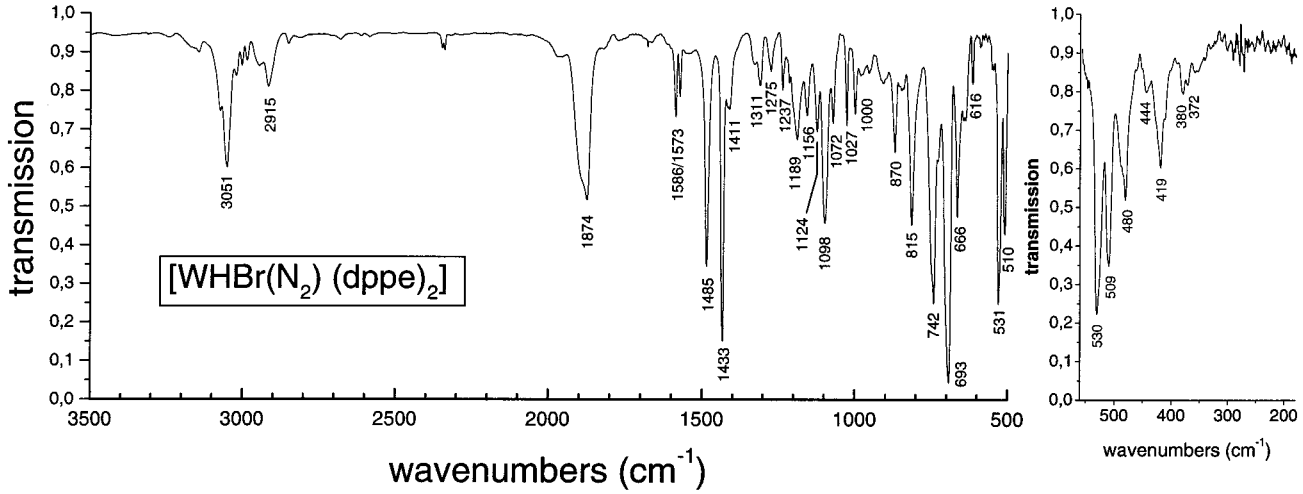

Figure 9. IR spectra of [WHBr(N$_2$)(dppe)$_2$] at 30 K. All peak positions in cm^{-1}. In the FIR region, the spectrum was recorded using a 12 μm Mylar beamsplitter with resolution set to 1 cm^{-1}.

the nondiagonal matrix elements H^{B}_{NN} and H_{MB}. The results of this procedure are listed in Table 5. For the three modes under investigation, good agreement with experimental data is achieved. The obtained force constants are listed in Table 4.

Discussion

In the present publication, the vibrational spectra of the two bis-dinitrogen complexes [M(N$_2$)$_2$(dppe)$_2$] (M = Mo (**Ia**), W (**Ib**)) and the protonated derivatives [WF(NNH)(dppe)$_2$] (**IIb**) and [WF(NNH$_2$)(dppe)$_2$](BF$_4$) (**IIIb**) have been investigated in detail for the first time. For **Ib** and **IIIb**, nearly all normal modes of the central N−N−W−N−N and F−W−N−NH$_2$ cores, respectively, have been identified making use of isotopic substitution. In case of **IIb**, the spectroscopic data are less informative. Nevertheless, the N−N stretch also could be assigned for this system. Based on the experimental data, a QCA-NCA has been carried out for **Ib** and **IIIb** and a complete set of force constants has been determined. A restricted QCA-NCA has been performed for **IIb** allowing an estimate of the most interesting force constants. This way, the vibrational

Table 5. Comparison of the Observed and Calculated Frequencies of [WF(NNH)(dppe)$_2$] (**IIb**) (in cm^{-1})

		experimental[b]			QCA-NCA		
mode	sym.[a]	NNH	^{15}N^{15}NH	NND	NNH	^{15}N^{15}NH	NND
ν(NH)	A′				3294	3287	2408
ν(NN)	A′	1457	1406	1419	1452	1411	1419
δ(NNH)	A′	1222	1208	984	1223	1207	984
ν(WN)	A′	(∼530)			530	515	521
δ(WNN)	A′	514	502		515	501	483
ν(WF)	A′	459	459	459	459	459	459
τ(NN)[c]	A″				490	476	483
τ(WN)[c]	A″				266	265	197
ν(WP)		223/189	223/189	223/189	∼250	∼250	∼250
			[WHF(N$_2$)(dppe)$_2$]				
ν(NN)		1846	1761	1847			
ν(WH)		1811	1813	(1302)			

[a] Symmetry labels according to C_s of **IIb′**. [b] Data from IR spectroscopy. [c] Both torsions are strongly mixed (nearly 1:1).

Chart 6. Definition of the Symmetry Coordinates of the Central F−W−N−NH Unit in [WF(NNH)P$_4$] (**IIb′**) in C_s[a]

$S_1^{A'} = r_6$	ν(WF)
$S_2^{A'} = r_7$	ν(WN)
$S_3^{A'} = r_{78}$	ν(NN)
$S_4^{A'} = r_{NH_9}$	ν(NH)
$S_5^{A'} = \beta_{WNN}$	δ(WNN)
$S_6^{A'} = \beta_{NNH}$	δ(NNH)
$S_1^{A''} = \tau_{WN-NH}$	τ(NN)
$S_2^{A''} = \tau_{P_4W-NN}$	τ(WN)

[a] The internal coordinates are defined in Figure 7.

Chart 7. Symbolic ***F*** Matrix of the Central F−W−N−NH Unit in [WF(NNH)P$_4$] (**IIb′**) in C_s Symmetry[a]

ν(WF) $A'^{(1)}$	ν(WN) $A'^{(2)}$	ν(NN) $A'^{(3)}$	ν(NH) $A'^{(4)}$	δ(WNN) $A'^{(5)}$	δ(NNH) $A'^{(6)}$	τ(NN) $A''^{(1)}$	τ(WN) $A''^{(2)}$
Y_1	N_t	N_SF	0	0	0	0	0
N_t	Y_2	N_S	H^S_{MN}	H^M_{MM}	H^B_{MN}	0	0
N_SF	N_S	Z	H^S_{NN}	H^M_{MN}	H^B_{NN}	0	0
0	H^S_{MN}	H^S_{NN}	H_S	H^M_{MH}	H_{SB}	0	0
0	H^M_{MM}	H^M_{MN}	H^M_{MH}	H_M	H_{MB}	0	0
0	H^B_{MN}	H^B_{NN}	H_{SB}	H_{MB}	H_B	0	0
0	0	0	0	0	0	T_1	T_{12}
0	0	0	0	0	0	T_{12}	T_2

[a] This short form of the matrix does not include the nondiagonal elements between ν(WF) and ν(WN) and the two symmetric ν_s(WP) combinations ($\sqrt{2}F_c1$; $\sqrt{2}F_c2$ and $\sqrt{2}N_c1$; $\sqrt{2}N_c2$, respectively) and the nondiagonal elements between δ(WNN) and the octahedral bends δ(PWF) ($\sqrt{2}\alpha_1$ and $\sqrt{2}\alpha_1'$) and δ(PWN) ($\sqrt{2}\beta_2$ and $\sqrt{2}\beta_2'$).

properties of the first intermediates of the asymmetric protonation pathway of dinitrogen have been determined.

The QCA-NCA procedure can be applied provided that the ab-initio force field is of sufficient quality. The merits of this method are twofold: (i) it is possible to include atoms or ligands (*frame*) in the NCA process, which influence the vibrations of the subunit under investigation (*core*), but the modes of which cannot be determined experimentally. For example, in case of the dinitrogen complex **Ib**, the frame of the four phosphorus atoms is very important for the vibrations of the N−N−W−N−N core, but only three W−P stretches and none of the in-plane (δ(PWP)) or out-of-plane bends (δ(PWN)) can be assigned from experiment. Therefore, an inclusion of this frame without the calculated force field would not be meaningful. Alternatively, omission of the frame may lead to serious errors regarding the modes of the core. This point has been discussed for the NCA we performed on a diazene complex of iron.[18] Therefore, QCA-NCA allows us to avoid crude simplifications in the models used for NCA. (ii) In addition, the QCA-NCA procedure makes the treatment of borderline cases as **IIb** possible where spectroscopic data are incomplete. The missing information can be supplied from the ab-initio force field. The success of the QCA-NCA procedure is striking: for **Ib** and **IIIb**, very good agreement with experiment has been achieved. Even in the case of **IIb**, a restricted QCA-NCA has been possible. This way, the results obtained with QCA-NCA are potentially superior to conventional NCA.

The vibrational frequencies of both N−N stretches $\nu_{s/as}$(NN) in various bis-dinitrogen complexes of type [M(N$_2$)$_2$(P)$_4$] (M = Mo, W) with different mono- and bidentate phosphine ligands have been repeatedly assigned.[5a,21,22] The literature values for compounds **Ib** and **Ia** are spread around the frequencies we have obtained. In contrast, assignments of other vibrations than $\nu_{s/as}$(NN) are rare: Colquhoun et al.[21] measured Raman spectra of both **Ib** and **Ia** but did not assign ν_s(MN) or δ_s(MNN). Instead, they present a number of different vibrations as possible candidates for one of these modes. In fact, the W−N stretch of **Ib** at 419/414 cm^{-1} is one of the peaks nominated in this work. On the other hand, the features listed for **Ia** do not include ν_s(MoN) at 393/(404) cm^{-1}, and the symmetric linear bends do not belong to any of the quoted features. Nevertheless, the assignment of ν_s(MP) (A_g) to peaks at 179 and 169 cm^{-1} for **Ib** and **Ia**, respectively, is in agreement with our results. In another study, Hussain et al.[5a] assigned ν_{as}(MN) in different bis-dinitrogen complexes to peaks at about 550 cm^{-1} from IR measurements. Most probably, however, these peaks belong to the corresponding antisymmetric bends δ_{as}(MNN) as observed for **Ib** and **Ia**. To date, force constants for W/Mo dinitrogen complexes have only been calculated for the N−N stretches[7] with simple two-dimensional models. Nevertheless, the obtained force constant of f_{NN} = 16.11 mdyn/Å for **Ib**[7b] is in good agreement with our QCA-NCA result.

The IR properties of different diazenido(−) complexes of type [MX(NNH)(dppe)$_2$] (M = Mo, W; X = halide) have been investigated by Chatt et al.[2d] They assigned ν(NN) to peaks at about 1800−1900 cm^{-1}; in case of **IIb**, to 1820 cm^{-1}. In contrast, monoalkylated systems [MX(NNR)(dppe)$_2$] (M = Mo, W; X = Cl$^-$, Br$^-$) exhibit N−N stretches of about 1500−1550

(20) α_1 and α_1' connect δ(WNN) to δ(PWF) (diagonal elements S_1 and S_1', respectively); β_2 and β_2' connect δ(WNN) to δ(PWN) (diagonal elements S_2 and S_2', respectively).

(21) Colquhoun, H. M.; Head, R. A. *Inorg. Chim. Acta* **1980**, *45*, L123.
(22) (a) George, T. A.; Seibold, C. D. *Inorg. Chem.* **1973**, *12*, 2544. (b) See ref 2b,e,f. (c) Chatt, J.; Hussain, W.; Leigh, G. J.; Neukomm, H.; Pickett, C. J.; Rankin, D. A. *J. Chem. Soc., Chem. Commun.* **1980**, 1024. (d) George, T. A.; Hayes, R. K.; Mohammed M. Y.; Pickett, C. J. *Inorg. Chem.* **1989**, *28*, 3269. (e) George, T. A.; DeBord, J. R. D.; Kaul, B. B.; Pickett, C. J.; Rose, D. J. *Inorg. Chem.* **1992**, *31*, 1295.

cm^{-1}.[23] This contradiction was commented on in a later paper,[19] and the intense peaks above 1800 cm^{-1} were attributed to corresponding metal-protonated species. Making use of isotope substituted compounds, we demonstrate that this hypothesis is correct. Moreover, we are able to assign the N−N stretching vibration to 1457 cm^{-1} in complex **IIb** which also contains traces of the metal-protonated species with ν(NN) at 1846 cm^{-1}. The N−H stretching vibration was assigned to a peak at 3365 cm^{-1} in **IIb** by Chatt et al.[2d] which shifts down to 2495 cm^{-1} on deuteration. However, we are not able to maintain this assignment because no corresponding feature is observed in the presented IR measurements. Maybe the peak at 3365 cm^{-1} is due to CH_3OH which sometimes appears in the IR spectra at about 3350 cm^{-1} and shifts below 2500 cm^{-1} on deuteration (cf. Figure 8).

For the double-protonated complexes $[MX(NNH_2)(P)_4]Y$ (M = Mo, W; X = halide; Y= halide, tetrafluoroborate, etc.), in most cases only the N-H stretching modes have been assigned;[9,24] the corresponding vibrations of **IIIb** are found at 3335 and 3255 cm^{-1}.[2d] Moreover, for some chloro and bromo compounds, the N−N−H bends have been assigned to peaks close to 1600 cm^{-1}.[2b] All these findings are in good agreement with our results. On deuteration, δ_s(NNH) was reported to shift to about 1370 cm^{-1}.[2b] This cannot be correct, because the predicted shift from QCA-NCA as well as ab-initio theory is nearly *twice as large*. We assign the corresponding feature at 1364 cm^{-1} in **IIIb** to ν(NN) in accordance with our NCA. Moreover, this is in agreement with results from IR spectroscopy obtained for the protonated monoalkylated complexes $[MX(NNHR)(dppe)_2]Y$ (M = Mo, W; X, Y = halide) according to which ν(NN) should appear in the region from 1300 to 1500 cm^{-1}.[23]

Force Constants of Mo/W−Nitrogenic Systems: Asymmetric Pathway. It is revealing to compare the N−N and W−N force constants of the three ligands N_2, NNH, and NNH_2 coordinated to tungsten as these compounds serve as models for the asymmetric reduction pathway of nitrogenase. In the bis-dinitrogen complex, the N−N bond is distinctly weakened (f_{NN} = 16.43) compared to free N_2 (f_{NN} = 22.42) and the W−N bond is quite strong (f_{WN} = 2.66). This is in agreement with the observed thermodynamic stability of the metal−N_2 bond in this compound. The first protonation extremely lowers the strength of the N−N bond leading to a force constant f_{NN} = 8.27 which is even lower than the ab-initio value for free isodiazene (11.7).[17] This strong reduction of f_{NN} can only originate from a significant flow of negative charge from the metal to the π* orbitals of N_2 going along with the protonation. As the NNH ligand has a lower N−N force constant than free NNH_2, it is best described as diazenido(−) in agreement with the common nomenclature. In contrast, the force constant of the W−N bond is increased to a value of $f_{WN} \sim 4.5$ indicating a significant strengthening of this bond as compared to the parent dinitrogen complex. A further increase of the metal−N bond order occurs upon the second protonation step (f_{WN} = 6.31). In accordance, the N−N force constant in the doubly protonated species is lowered to 7.20 which is of comparable magnitude as calculated for diazene bound to an iron complex (f_{NN} = 7.73).[18] Therefore, the coordinated NNH_2 ligand is best described as isodiazene in contrast to the usual hydrazido(2−) formulation. The described evolution of force constants reflects the salient feature of the asymmetric reduction pathway: on addition of each proton, the N−N bond order decreases, whereas the corresponding metal−N bond strength increases. This compensates for the thermodynamic unfavorable weakening of the N−N bond and serves to bind the partly reduced intermediate species even tighter to the metal.

Is there a connection between the N−N force constant of terminal end-on bound dinitrogen and its activation towards protonation? For the end-on terminally coordinating systems, activation is determined by a buildup of negative charge at the β-nitrogen atom. This is achieved by back-donation from the metal into both π* orbitals of N_2 which also leads to a lowering of the N−N bond strength. In that sense, the N−N force constant is a measure of both back-donation and activation. Empirically, if f_{NN} is in the magnitude of 18 mdyn/Å or even larger as observed for dinitrogen complexes of iron or ruthenium,[7b,14] protonation is improbable because back-donation is too weak. The reverse conclusion, however, is not true, because also complexes with a smaller N−N force constant than 18 mdyn/Å may not be protonable on the coordinated N_2. This indicates that protonation also depends on the stabilization of the resulting intermediates. In addition, side reactions may occur, for example metal protonation, as observed for a number of Re(I) complexes.[25] In the following paper, the end-on protonation pathway is investigated from an electronic structure point of view and the conditions both with respect to activation and the stabilization of intermediates are evaluated.

Acknowledgment. F.T. gratefully acknowledges the support of these investigations by the Deutsche Forschungsgemeinschaft (Grant Tu58/5-1) and Fonds der Chemischen Industrie (FCI) and thanks Dr. R. L. Richards, Nitrogen Fixation Laboratory, John Innes Center, Norwich (U.K.) for a sample of $[WHBr(N_2)(dppe)_2]$. In particular, preparative work of N. Böres is gratefully acknowledged. N.L. thanks FCI for a Kekulé Research Fellowship. We thank the Emil und Paul Müller Gedächtnisstiftung, Universität Mainz, for financial aid.

IC980939+

(23) (a) Day, V. W.; George, T. A.; Iske, S. D. A. *J. Am. Chem. Soc.* **1975**, *97*, 4127. (b) Chatt, J.; Diamantis, A. A.; Heath, G. A.; Hooper, N. E.; Leigh, G. J. *J. Chem. Soc., Dalton Trans.* **1977**, 688. (c) Bevan, P. C.; Chatt, J.; Diamantis, A. A.; Head, R. A.; Heath, G. A.; Leigh, G. J. *J. Chem. Soc., Dalton Trans.* **1977**, 1711. (d) Bossard, G. E.; Busby, D. C.; Chang, M.; George, T. A.; Iske, S. D. A., Jr. *J. Am. Chem. Soc.* **1980**, *102*, 1001. (e) Busby, D. C.; George, T. A.; Iske, S. D. A., Jr.; Wagner, S. D. *Inorg. Chem.* **1981**, *20*, 22.

(24) See refs 2b,d,g,h,i,k,l.

(25) Chatt, J.; Dilworth, J. R.; Leigh, G. J. *J. Chem. Soc., Dalton Trans.* **1973**, 612.